Magnetic structure evolution of $NdMnO_3$ derived from neutron diffraction data

J. Phys.: Condens. Matter **12** (2000) 1361–1376. Printed in the UK PII: S0953-8984(00)05141-9

Magnetic structure evolution of $NdMnO_3$ derived from neutron diffraction data

A Muñoz†¶, J A Alonso‡, M J Martínez-Lope‡, J L García-Muñoz§ and M T Fernández-Díaz‖

† Departamento de Física, EPS, Universidad Carlos III, Avenida de la Universidad 30, Leganés, E-28911 Madrid, Spain
‡ Instituto de Ciencia de Materiales de Madrid, CSIC, Cantoblanco, E-28049 Madrid, Spain
§ Instituto de Ciencia de Materiales de Barcelona, CSIC, Bellaterra, E-28193 Barcelona, Spain
‖ Institut Laue–Langevin, BP 156X, 38042 Grenoble Cédex 9, France

E-mail: amunoz@elrond.uc3m.es

Received 14 June 1999, in final form 11 November 1999

Abstract. The orthorhombic $NdMnO_3$ perovskite (space group $Pnma$) has been studied on the basis of magnetization and neutron powder diffraction (NPD) data. Magnetization measurements suggest the coexistence of ferromagnetic and antiferromagnetic interactions: magnetization versus magnetic field curves present a remnant magnetization in the ordered region, which is around 1 μ_B at $T = 6$ K. The thermal evolution of the magnetic structure has been followed down to 1.5 K from the NPD data. These measurements show that the Mn sub-lattice becomes ordered below $T_N \approx 78$ K with a spin arrangement $(C_x, F_y, 0)$, in such a way that a ferromagnetic component appears along the y-direction. The Nd sub-lattice becomes ordered below $T \approx 13$ K according to a ferromagnetic arrangement with the moments parallel to the y-direction. At $T = 1.5$ K the magnetic moment values are 3.22(9) μ_B for Mn atoms and 1.2(2) μ_B for Nd atoms.

1. Introduction

The observation of a colossal magnetoresistance effect in rare-earth manganite $R_{1-x}A_xMnO_3$ (R = lanthanides, A = Ba, Sr, Ca) thin films [1–3] has triggered an intense effort to correctly characterize these fascinating systems, some of the properties of which (magnetic ordering, charge ordering, charge disproportionation) have not been completely understood yet. In fact, the magnetic properties of the parent $RMnO_3$ oxides were first studied a long time ago, and it was then established that the low-temperature ground state of $RMnO_3$ is antiferromagnetic [4–6]. It was also known that when substituting Sr for La in the perovskite $LaMnO_3$ the ground state becomes ferromagnetic and the magnetic transition from the paramagnetic state to the magnetically ordered state is accompanied by a very strong drop in the resistivity [4]. Recently, it was discovered that, in $Nd_{0.5}Sr_{0.5}MnO_3$ [7] and $Pr_{1-x}Ca_xMnO_3$ [8, 9], a similar sharp drop in the resistivity can be induced by the application of a magnetic field.

All of these mixed-valence manganites are based on the parent $RMnO_3$ perovskites. For rare-earth cations from La to Dy, $RMnO_3$ perovskites are orthorhombically distorted and the crystal structure is described in the space group $Pnma$ [10]. In spite of the exhaustive studies carried out on $R_{1-x}A_xMnO_3$ manganites, comparatively little work has been done

¶ Author to whom any correspondence should be addressed.

0953-8984/00/071361+16$30.00

on stoichiometric (undoped) $RMnO_3$ compounds. As regards the low-temperature magnetic structures, they have been described for a limited number of compounds. Neutron diffraction experiments performed on $LaMnO_3$ [11–13] showed that its magnetic structure, defined by the propagation vector $\boldsymbol{k} = 0$, is C_x (space group $Pnma$). The magnetic structures of $PrMnO_3$ and $NdMnO_3$ were also studied [14]. For both compounds the magnetic unit cell coincides with the chemical one, and the magnetic structure is C_x for $PrMnO_3$ and C_xC_y for $NdMnO_3$ (space group $Pnma$). In both cases the magnetic ordering only concerns the Mn sub-lattice. However, for $NdMnO_3$ the antiferromagnetic structure is at variance with the magnetic behaviour found by Pauthenet and Veyret [6], since the isothermal magnetization measurements present a remnant magnetization at low temperature. The magnetic structure of $TbMnO_3$ has also been determined [15], and it was shown to be incommensurate. Firstly, Mn atoms order according to a sine-wave magnetic structure and, at lower temperature, Tb atoms also order, but according to a different modulated sine-wave structure. The magnetic structures of the rest of the $RMnO_3$ compounds have not yet been analysed, although magnetic measurements were carried out on some of them, such as $EuMnO_3$ [16] and $GdMnO_3$ [17]. They seem to show that, firstly, the Mn sub-lattice orders and that, at lower temperature, the rare-earth sub-lattice ordering would be responsible for the weak magnetism observed. In this paper the magnetic structure of $NdMnO_3$ is revisited; in particular we describe its thermal evolution and the unexpected ordering of the Nd sub-lattice at low temperature. A refinement of the crystallographic structure from high-resolution NPD data is also included.

2. Experimental procedure

Black polycrystalline powder of $NdMnO_3$ was prepared from stoichiometric amounts of analytical-grade Nd_2O_3 and $MnCO_3$, which were dissolved in citric acid by adding several droplets of concentrated HNO_3. The citrate + nitrate solutions were slowly evaporated, leading to an organic resin containing a random distribution of the cations involved at an atomic level. The resin was first dried at 120 °C, then ground and slowly decomposed at temperatures up to 600 °C. All the organic materials and nitrates were eliminated in a subsequent treatment at 700 °C in air, for 12 hours. A final treatment at 1000 °C, in air, followed by quenching of the sample to room temperature, yields a pure perovskite phase with excellent crystallinity.

Magnetic measurements were performed on a PPMS (Quantum Design) system by the extraction method. The expected sensitivity of the system is 2.5×10^{-5} emu. The thermal dependence of the magnetization was measured in a temperature range from 1.5 K to 350 K at $H = 0.2$ T and $H = 3$ T. Isothermal magnetization curves were obtained at several temperatures, 6, 40 and 100 K, and in magnetic fields ranging from −35 kOe to 35 kOe. Neutron powder diffraction (NPD) diagrams were collected at the Institut Laue–Langevin in Grenoble (France) at the D2B and D20 diffractometers. To refine the crystallographic structure, a high-resolution diagram was acquired at room temperature (D2B) with a wavelength $\lambda = 1.594$ Å. The thermal evolution of the NPD patterns was followed at D20 with a longer wavelength, $\lambda = 2.532$ Å, in the temperature range from 1.5 K to 300 K. The data were analysed by the Rietveld method [18] and the refinements of both the crystallographic and the magnetic structure were performed with the program FULLPROF [19]. In the refinements the peak shape was described by a pseudo-Voigt function and the background was fitted with a fifth-degree polynomial function. The Fermi scattering lengths for Nd, Mn and O were 7.690, −3.730 and 5.803 fm, respectively. The magnetic form factors used for the Nd and Mn atoms were determined with the coefficients taken from the *International Tables* [20].

3. Results from magnetization measurements

The thermal evolution of the magnetization is presented in figure 1. At low temperature, both the zero-field-cooled (ZFC) and the field-cooled (FC) magnetization curves measured in a field of $H = 2$ kOe are characteristic of an antiferromagnetic behaviour with maxima at $T \approx 60$ K and $T \approx 37$ K, respectively. However, the hysteresis observed in both curves below 80 K suggests the presence of a ferromagnetic component. The presence of a ferromagnetic component is confirmed by the magnetization versus magnetic field measurements shown in figure 2. In the isothermal magnetization curve corresponding to $T = 6$ K a remnant magnetization is observed, its value being around 1 μ_B per formula. Although a small remnant magnetization is still observed at $T = 40$ K, around 0.1 μ_B per formula, at $T = 100$ K the field dependence of the magnetization is linear and no hysteresis is observed, which reveals a paramagnetic behaviour.

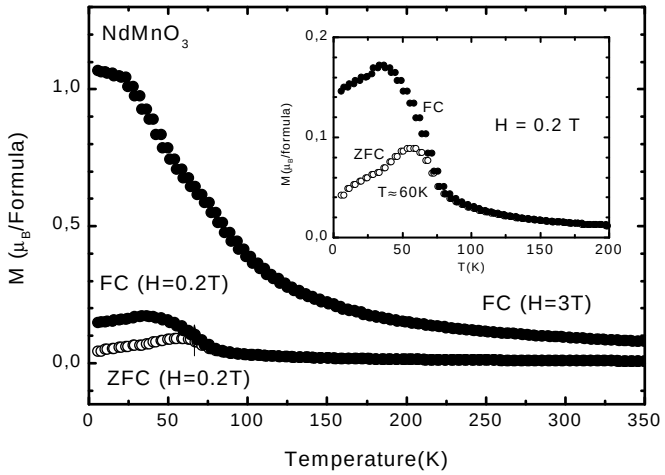

Figure 1. The temperature dependence of the zero-field-cooled and field-cooled magnetization in different magnetic fields for $NdMnO_3$. Inset: an enlargement at low temperature.

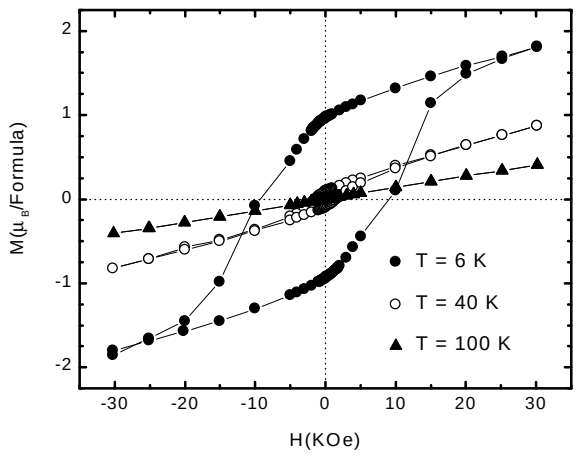

Figure 2. Magnetization versus magnetic field for $NdMnO_3$ at different temperatures.

The thermal variation of the reciprocal susceptibility is shown in figure 3. A linear behaviour is observed above 100 K, which suggests a Curie–Weiss behaviour. However, a curvature appears between 250 K and 300 K, after which a linear behaviour is again observed. From the data between 100 K and 250 K a paramagnetic temperature $\Theta_P = -37$ K has been obtained. This negative value implies the presence of antiferromagnetic interactions. The effective paramagnetic moment is 6.48 μ_B per formula. This value is slightly higher than the theoretical value calculated as

$$\mu_{eff} = ((\mu_{Mn^{3+}})^2 + (\mu_{Nd^{3+}})^2)^{1/2} = 6.20\ \mu_B$$

where the values $\mu_{Mn^{3+}} = 4.9\ \mu_B$ for Mn^{3+} (spin only) and $\mu_{Nd^{3+}} = 3.8\ \mu_B$ for Nd^{3+} ($J = \frac{9}{2}$) have been taken. If the temperature range 300–350 K is considered, an effective paramagnetic moment of 6.22 μ_B is obtained, very close to the expected value.

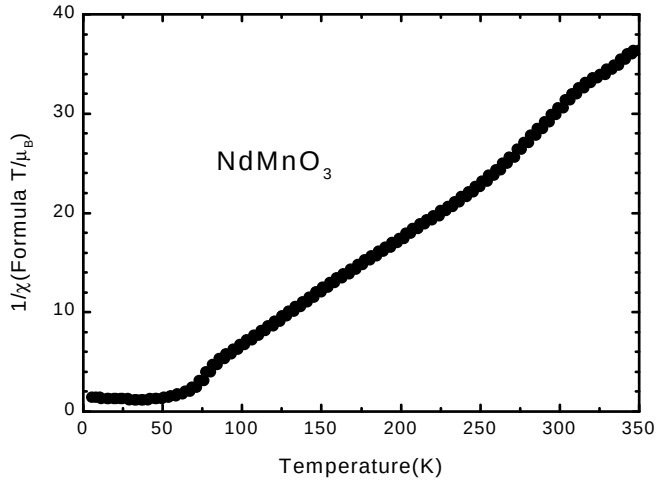

Figure 3. Thermal variation of the reciprocal of the susceptibility for $NdMnO_3$.

4. Results from NPD measurements

4.1. Crystal structure refinements

A NPD pattern collected at room temperature with $\lambda = 1.594$ Å was used for the refinement of the $NdMnO_3$ crystallographic structure. All of the Bragg reflections of the diffraction diagram can be indexed in the orthorhombic space group *Pnma* with the unit-cell parameters $a = 5.7119(9)$ Å, $b = 7.5890(13)$ Å and $c = 5.4119(8)$ Å. As rare-earth deficiency in $RMnO_3$ perovskites has been described, the occupancy factor of Nd atoms was allowed to vary in the first stages of the refinement. It converged to 0.99(1), so no appreciable Nd non-stoichiometry is detected from NPD data. The good agreement between the observed and calculated patterns is shown in figure 4.

The structural parameters calculated in the refinement are presented in table 1.

In the MnO_6 octahedra the average Mn–O distances are close to the sum of the ionic radii, although the individual distances reveal a rather strong Jahn–Teller distortion of the octahedra, with bond lengths in the range 1.927(3) to 2.132(3) Å. The rather bent Mn–O–Mn bonding angles correspond to a severe distortion of the perovskite structure (see table 2).

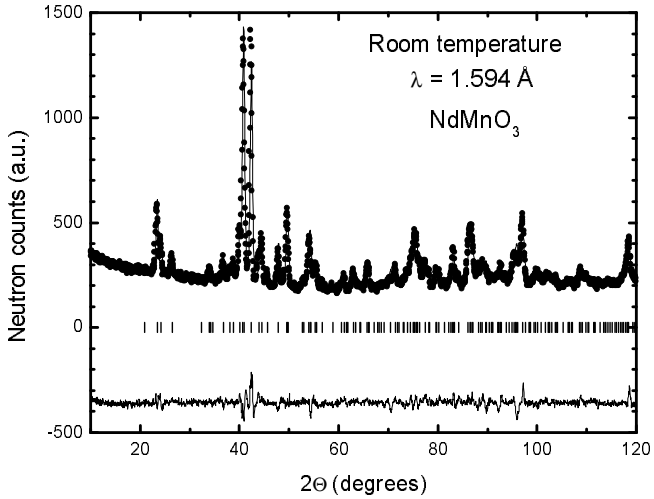

Figure 4. Observed (●) and calculated (——) neutron diffraction patterns at room temperature. Bragg reflections are indicated by tick marks. The difference between the observed and calculated pattern is also plotted.

Table 1. Structural parameters obtained in the Rietveld refinement of the NPD pattern at room temperature and with $\lambda = 1.594$ Å. Space group: *Pnma*.

Atoms	*x*	*y*	*z*	*B* (Å^2)
Nd 4c	0.0597(7)	0.2500	0.9909(9)	0.87(8)
Mn 4b	0.0000	0.0000	0.5000	0.10(10)
O1 4c	0.4837(8)	0.2500	0.0817(8)	0.67(10)
O2 8d	0.3106(6)	0.0405(4)	0.7108(6)	0.78(9)
Cell (Å)	$a = 5.7119(9)$	$b = 7.5890(13)$	$c = 5.4119(8)$	Volume = 234.60(11) Å^3
Discrepancy factors	$R_p = 4.4\%$	$R_{wp} = 5.8\%$	$R_B = 6.8\%$	$\chi^2 = 2.7$

Table 2. Selected interatomic distances (in Å) and angles (in degrees).

Mn distances		Nd distances	
Mn–O1 (×2)	1.950(1)	Nd–O1	2.353(6)
Mn–O2 (×2)	1.927(3)	Nd–O1	2.471(6)
Mn–O2 (×2)	2.132(3)	Nd–O2 (×2)	2.397(5)
⟨Mn–O⟩	2.003(1)	Nd–O2 (×2)	2.613(4)
∑Radii	2.016	Nd–O2 (×2)	2.623(5)
Mn–Mn (×2)	3.7945(6)	⟨Nd–O⟩	2.511(2)
Mn–Mn (×4)	3.9342(4)	∑radii	2.480
Mn–O–Mn angles			
Mn–O1–Mn	153.20(5)		
Mn–O2–Mn (×2)	151.50(14)		

As regards Mn–Mn distances, the distance from a Mn atom to its four nearest neighbours in the same $(0, y, 0)$ plane, $d = 3.9342(4)$ Å, is higher than the distance to its two closest neighbours in different $(0, y, 0)$ planes, $d = 3.7945(6)$ Å. This fact will play an important role in the magnetic interactions between Mn atoms.

4.2. Magnetic structure determination

4.2.1. Low-temperature neutron diffraction. Figure 5 shows the thermal variation of NPD patterns collected at low temperature.

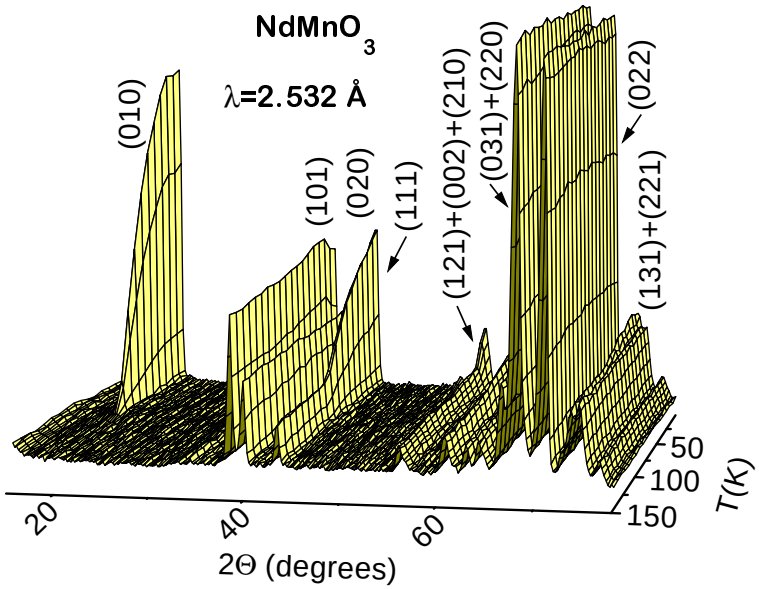

Figure 5. Thermal evolution of NPD patterns collected at a wavelength $\lambda = 2.532$ Å in the temperature range 1.5 K–150 K.

(This figure can be viewed in colour in the electronic version of the article; see `www.iop.org`)

On decreasing the temperature, from the pattern acquired at $T = 77.6$ K some changes are observed in certain Bragg reflections: on the one hand, some Bragg reflections forbidden by the space group $Pnma$, such as the (010) reflection, start to be observed and, on the other hand, some permitted reflections, such as the (111) reflection, increase in intensity. This corresponds to the onset of a magnetic ordering in good agreement with [14]. As magnetic peaks do not appear at positions different from Bragg reflections, the magnetic unit cell coincides with the chemical one. The thermal evolutions of the integrated intensities corresponding to the most important magnetic reflections are presented in figures 6 and 7.

From a detailed analysis of the different patterns it is found that (hkl) reflections with h and l of different parity do not exhibit any change in the ordered region. Initially only (hkl) magnetic reflections with k odd and $h + l = 2n$ are observed; however, as temperature decreases, some reflections with k even and $h + l = 2n$ also appear to have a magnetic contribution. When temperature decreases below 13 K a remarkable change in the intensity of some magnetic peaks is observed. The peak formed by the reflections (121), (002) and (210) and the reflection (200) increases (see figure 7). On the other hand, the peak formed by the reflections (101) and (020) presents a significant decrease in its integrated intensity (see figure 7). As the rest of the observed magnetic reflections increase progressively their intensity and new reflections are not observed, we expect some minor changes in the magnetic structure, like, for instance, the ordering of another magnetic atom with a magnetic arrangement defined by the same propagation vector $\boldsymbol{k} = 0$.

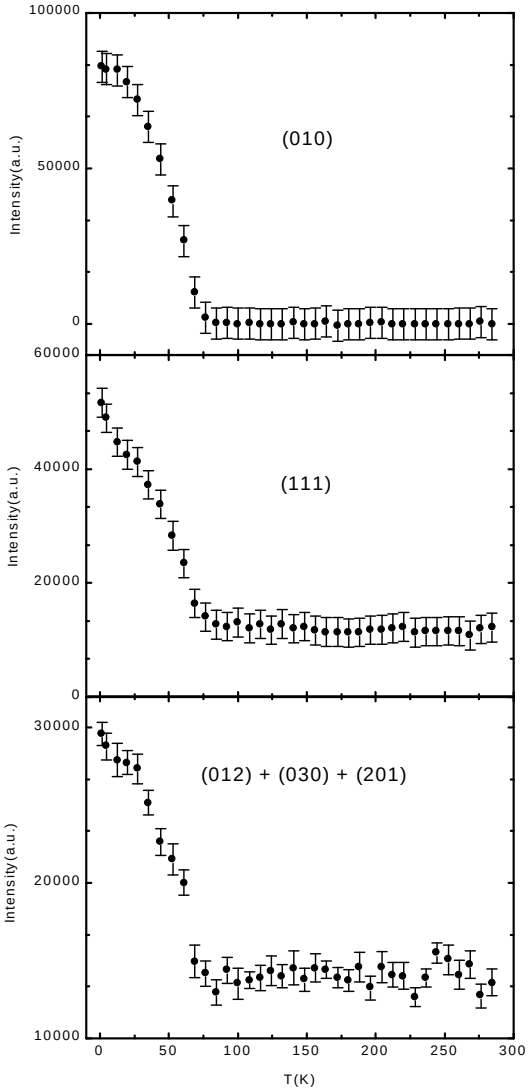

Figure 6. Thermal evolution of the magnetic reflections (010), (111) and (012) + (030) + (201) in the temperature range 1.5–300 K.

4.2.2. Group theory analysis. The possible magnetic modes compatible with the crystal symmetry have been obtained by following the method described by Bertaut [21]. For $\boldsymbol{k} = 0$ the little group, G_k, coincides with the space group $Pnma$. The Γ representation constructed with the magnetic moments of the four Mn atoms corresponding to the 4b site decomposes in terms of the eight irreducible representations of the space group $Pnma$ as

$$\Gamma_{\mathrm{Mn}} = 3(\Gamma_1 + \Gamma_3 + \Gamma_5 + \Gamma_7).$$

For the four Nd atoms of the 4c site the decomposition is

$$\Gamma_{\mathrm{Nd}} = (\Gamma_1 + \Gamma_4 + \Gamma_5 + \Gamma_8) + 2(\Gamma_2 + \Gamma_3 + \Gamma_6 + \Gamma_7).$$

The basis vectors obtained for each irreducible representation Γ_i according to the projection operator method are reported in table 3.

Let us point out that the extinction rules for the Mn-sub-lattice contribution to the magnetic structure factor are the following ones. For the magnetic modes $\boldsymbol{F}$ and $\boldsymbol{G}$ the only (hkl)

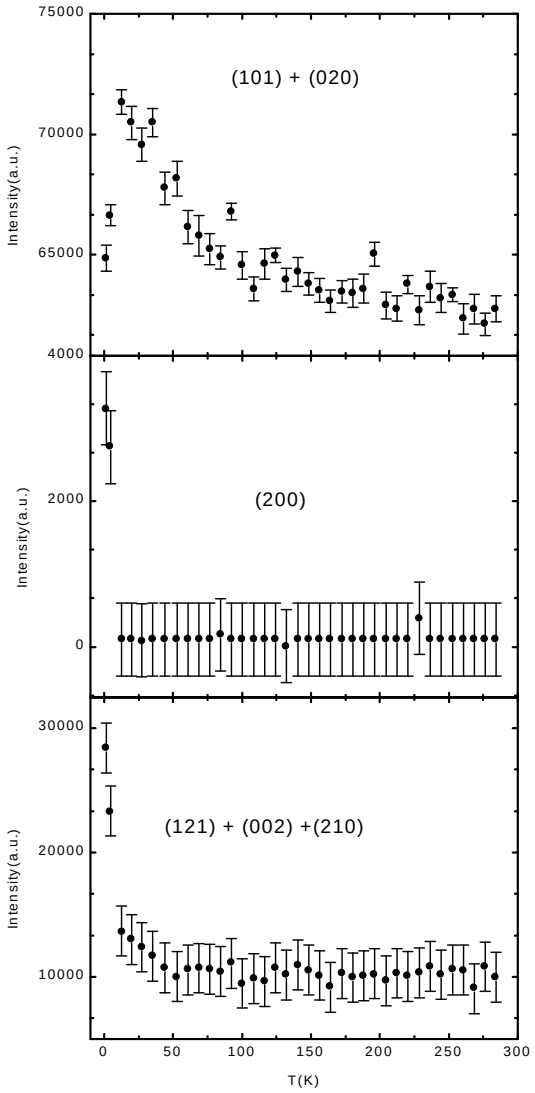

Figure 7. Thermal evolution of the magnetic reflections (101) + (020), (200) and (121) + (002) in the temperature range 1.5–300 K.

permitted reflections are those with k even plus $h + l = 2n$ for the mode $\boldsymbol{F}$ and $h + l = 2n + 1$ for the mode $\boldsymbol{G}$. On the other hand, for the modes $\boldsymbol{C}$ and $\boldsymbol{A}$ the permitted reflections are those with k odd plus $h + l = 2n$ for the mode $\boldsymbol{C}$ and $h + l = 2n + 1$ for the mode $\boldsymbol{A}$.

4.2.3. Magnetic structure refinement. All NPD diagrams collected in the ordered region at $\lambda = 2.532$ Å have been considered in the determination of the magnetic structure. In the temperature range from 13 K to 77.6 K the best agreement with the experimental data is achieved by considering that only the Mn sub-lattice is ordered. In this temperature range, magnetic reflections with $h + l = 2n + 1$ are not observed, which implies that the magnetic modes $\boldsymbol{A}$ and $\boldsymbol{G}$ cannot take part in the solution. So the only possible solutions would be $(0, 0, C_z)$, $(F_x, C_y, 0)$, $(C_x, F_y, 0)$ and $(0, 0, F_z)$, which are associated with the irreducible representations Γ_1, Γ_3, Γ_5 and Γ_7, respectively (see table 3). After checking all of these solutions, it is found that the best agreement is obtained for $(C_x, 0, 0)$ and $(C_x, F_y, 0)$. In table 4

Table 3. Basis vectors for $G = Pnma$ and $\boldsymbol{k} = 0$. Atomic positions: for Mn, Mn1 $(0, 0, \frac{1}{2})$, Mn2 $(\frac{1}{2}, 0, 0)$, Mn3 $(0, \frac{1}{2}, \frac{1}{2})$, Mn4 $(\frac{1}{2}, \frac{1}{2}, 0)$; for Nd, Nd1 $(x, \frac{1}{4}, z)$, Nd2 $(\overline{x}+\frac{1}{2}, \frac{3}{4}, z+\frac{1}{2})$, Nd3 $(\overline{x}, \frac{3}{4}, \overline{z})$, Nd4 $(x+\frac{1}{2}, \frac{1}{4}, \overline{z}+\frac{1}{2})$.

	Mn(4b)	Nd(4c)
Γ_1	(A_x, G_y, C_z)	$(-, G_y, -)$
Γ_2	—	$(A_x, -, C_z)$
Γ_3	(F_x, C_y, G_z)	$(F_x, -, G_z)$
Γ_4	—	$(-, C_y, -)$
Γ_5	(C_x, F_y, A_z)	$(-, F_y, -)$
Γ_6	—	$(C_x, -, A_z)$
Γ_7	(G_x, A_y, F_z)	$(G_x, -, F_z)$
Γ_8	—	$(-, A_y, -)$
	$\boldsymbol{F} = \boldsymbol{m}_1 + \boldsymbol{m}_2 + \boldsymbol{m}_3 + \boldsymbol{m}_4$	$\boldsymbol{A} = \boldsymbol{m}_1 - \boldsymbol{m}_2 - \boldsymbol{m}_3 + \boldsymbol{m}_4$
	$\boldsymbol{G} = \boldsymbol{m}_1 - \boldsymbol{m}_2 + \boldsymbol{m}_3 - \boldsymbol{m}_4$	$\boldsymbol{C} = \boldsymbol{m}_1 + \boldsymbol{m}_2 - \boldsymbol{m}_3 - \boldsymbol{m}_4$

Table 4. Observed and calculated integrated intensities in the angle range $2\Theta = 16$–88° at $T = 21$ K and observed integrated intensities at $T = 94$ K. Only the Mn sub-lattice is ordered.

	I_{observed} $T = 94$ K	I_{observed} $T = 21$ K	$I_{\text{calculated}}$ $(C_x, 0, 0)$	$I_{\text{calculated}}$ $(C_x, C_y, 0)$	$I_{\text{calculated}}$ $(C_x, F_y, 0)$
(010)	No observation	1634(4)	1607	1612	1616
(100)	No observation	0	0	0	0
(001)	No observation	0	0	0	0
(110)	No observation	0	0	0	0
(011)	20(40)	25(40)	5	5	5
(101), (020)	1344(8)	1450(7)	1348	1348	1407
(120)	No observation	0	0	0	0
(021)	No observation	0	0	0	0
(200)	0(40)	0(23)	4	4	19
(121), (002), (210)	215(15)	334(9)	251	248	287
(012), (030), (201)	359(7)	678(7)	754	755	753
(102)	243(6)	251(6)	222	222	221
(211)	331(5)	318(5)	315	315	313
(112), (130), (031), (220)	4930(4)	4913(4)	4935	4935	4911
(022)	3740(3)	3754(3)	3693	3694	3678
(131), (221)	1127(4)	1358(4)	1324	1322	1318
(122)	230(6)	234(6)	225	225	223
(202)	773(5)	796(5)	857	857	861
(300), (212), (040), (230)	1671(4)	1800(4)	1779	1778	1770

the observed and calculated integrated magnetic intensities are compared for both models at $T = 21$ K. The results corresponding to the solution proposed by Quezel-Ambrunaz [14], $(C_x, C_y, 0)$, are also included. However, this last solution, which implies a mixture of magnetic modes belonging to two different irreducible representations, gives a result very similar to that for $(C_x, 0, 0)$. The fitting for $(C_x, C_y, 0)$ gives a y-component of the magnetic moment very close to zero, for instance, 0.20(15) μ_B at $T = 21$ K (see table 5).

Table 5. Discrepancy factors associated with the different models for $T = 21$ K.

$T = 21$ K Solution	Mn $(C_x, 0, 0)$	Mn $(C_x, C_y, 0)$	Mn $(C_x, F_y, 0)$
m_x	2.78(3)	2.80(3)	2.80(3)
m_y	—	−0.20(15)	−1.08(12)
$\|m\|$	2.78(3)	2.81(4)	3.00(7)
R_{Bragg}	3.80	3.80	3.40
χ^2	1.30	1.30	1.30

As regards the model $(C_x, 0, 0)$, in spite of the good values of the agreement factors of the refinement, some discrepancies are observed in the peak formed by the (101) and (020) reflections. Although the deviations between the observed and calculated integrated intensities do not seem to be important (see table 4), the thermal evolution of this reflection presented in figure 7 seems to show that a magnetic contribution exists in this reflection. According to the extinction rules corresponding to the $\boldsymbol{C}$-mode (k is even) no magnetic contribution should be observed in this reflection. In contrast, for the solution $(C_x, F_y, 0)$ the agreement between the observed and calculated integrated intensities for the peak formed by the (101) and (020) reflections is better, as the extinction rules for the $\boldsymbol{F}$-mode allow for a magnetic contribution to this peak. Thus, as the agreement with the rest of the reflections is good, this solution is preferred. The corresponding magnetic structure is reported in figure 8.

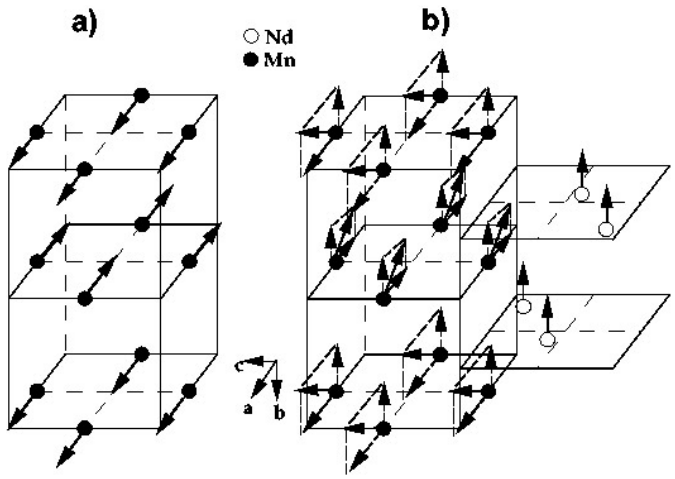

Figure 8. Magnetic structure for $NdMnO_3$. (a) For $65 < T < 78$ K only the Mn sub-lattice is ordered and its structure is C_x. (b) For $T < 13$ K both the Mn and Nd sub-lattices are ordered.

Therefore, there is a ferromagnetic component along the y-direction and, as regards the x-component, the magnetic structure consists of a stacking of ferromagnetic planes anti-ferromagnetically coupled along the b-direction. As is shown in figure 9, where the thermal

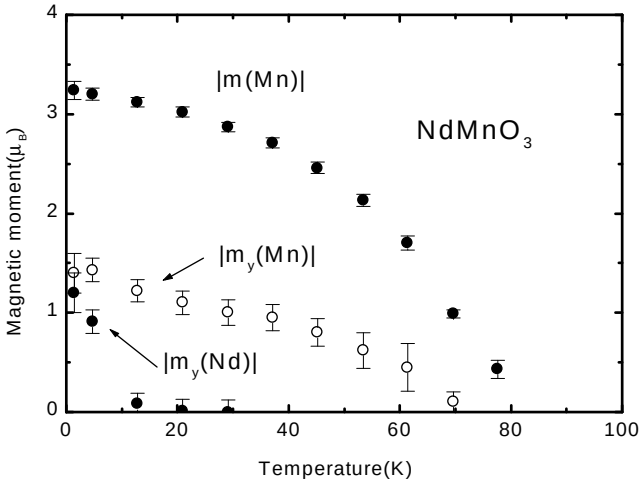

Figure 9. Thermal evolution of the magnetic moment for $NdMnO_3$.

variation of the magnetic moment is plotted, the ferromagnetic y-component appears at lower temperatures (by 15–20 K) than the ordering temperature, increasing its value as the temperature decreases. At $T = 21$ K the ferromagnetic component for the Mn atoms is $-1.08(12)$ μ_B and the total magnetic moment is 3.00(7) μ_B. The most important features of the magnetic structure refinement are reported in table 5 and the good agreement between the observed and calculated NPD patterns at $T = 21$ K is shown in figure 10.

Below $T = 13$ K, the changes observed in the NPD diagrams can be explained by assuming magnetic ordering of the Nd sub-lattice. Although the possibility that Nd atoms become ordered independently from Mn atoms was checked, the best solution was found when the magnetic structure of Nd moments is also given by the basis vectors of the same irreducible representation, Γ_5. Therefore, the solution is $(C_x, F_y, 0)$ for the Mn atoms and $(0, F_y, 0)$ for the Nd atoms. It corresponds to a ferromagnetic arrangement of the magnetic moments of the Nd atoms along the y-direction. As the changes only affect some of the magnetic reflections, mainly the reflections (101) + (020), (200) and (121) + (002) + (210) (see figure 7), the results for the solution are compared with those for the other three solutions considered before in the temperature range 13–77.6 K. In particular, the refinements carried out at $T = 1.5$ K are shown in table 6. The discrepancy factors and the calculated magnetic moments are presented in table 7. As can be seen in table 6, only the solution $(C_x, F_y, 0)$ for the Mn atoms and $(0, F_y, 0)$ for the Nd atoms can explain the changes observed in the reflections (200) and (121) + (002) + (210). For this solution, the good agreement between the observed and calculated patterns can be seen in figure 10 at $T = 1.5$ K. A plot of the magnetic structure found below 13 K is presented in figure 8. The thermal variation of the magnetic moment of the Nd atoms is presented in figure 9.

The Nd magnetic moment is enhanced as temperature decreases and at $T = 1.5$ K it achieves a value of 1.2(2) μ_B. For Mn atoms, at $T = 1.5$ K the magnetic moment value is 3.22(9) μ_B. The thermal evolution of the lattice parameters has also been determined (see figure 11). An anomaly is observed in both the a- and c-parameters at around 70 K, very close of the ordering temperature, which according to the neutron diffraction results is around $T_N \approx 78$ K, The relationship $b/\sqrt{2} \leqslant c \leqslant a$ is always obeyed, as also happens for $LaMnO_3$. This is characteristic of the so-called O′ structure and it originates from the strong cooperative

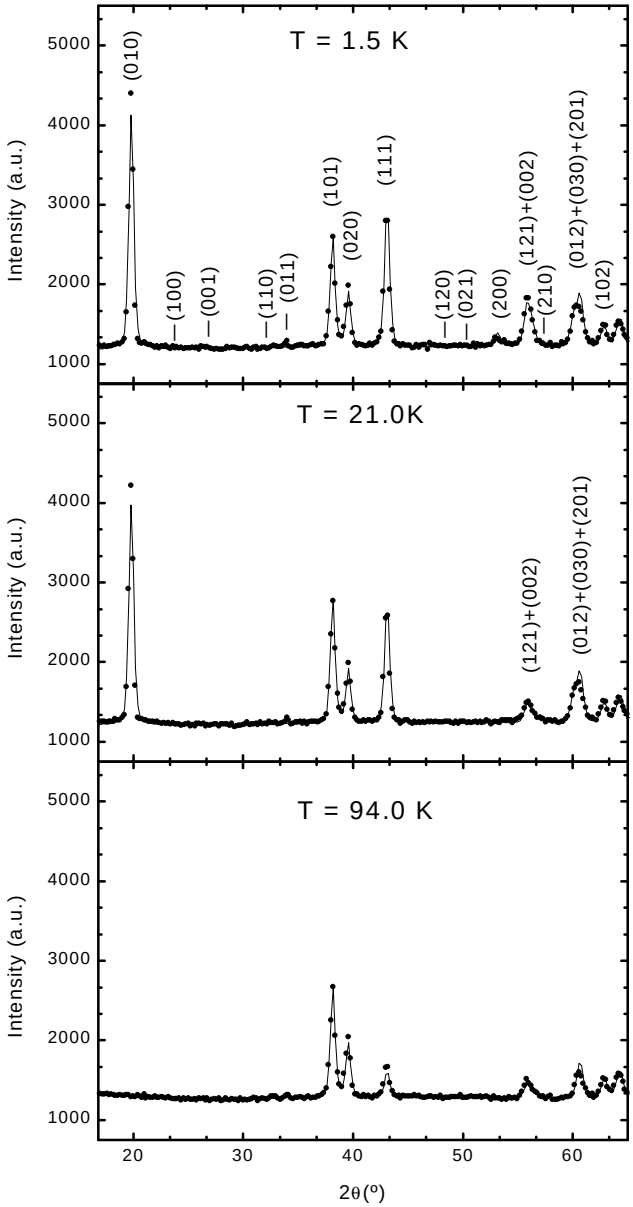

Figure 10. Observed (●) and calculated (solid line) neutron diffraction patterns at $T = 94$ K, $T = 21$ K and $T = 1.5$ K.

Jahn–Teller effect, inducing an orbital ordering and distorting the MnO_6 octahedra. This is in contrast with the usual situation in perovskites where the primary distorting effect is steric and $b/\sqrt{2}$ lies between c and a.

5. Discussion

In the magnetization versus magnetic field measurements a remnant magnetization is observed at $T = 6$ K, which is in good agreement with the magnetic structure determined from NPD data: in the low-temperature magnetic structure a ferromagnetic component develops along

Table 6. Observed and calculated integrated intensities in the angle range $2\Theta = 16$–88° at $T = 1.5$ K and observed integrated intensities at $T = 94$ K.

	I_{observed} $T = 94$ K	I_{observed} $T = 1.5$ K	$I_{\text{calculated}}$ Mn$(C_x, 0, 0)$	$I_{\text{calculated}}$ Mn$(C_x, C_y, 0)$	$I_{\text{calculated}}$ Mn$(C_x, F_y, 0)$	$I_{\text{calculated}}$ Mn$(C_x, F_y, 0)$, Nd$(0, F_y, 0)$
(010)	No observation	1741(4)	1751	1774	1767	1712
(100)	No observation	No observation	0	0	0	0
(001)	No observation	No observation	0	0	0	0
(110)	No observation	No observation	0	0	0	0
(011)	20(40)	30(40)	5	5	5	5
(101) (020)	1344(8)	1351(6)	1325	1301	1439	1339
(120)	No observation	No observation	0	0	0	0
(021)	No observation	No observation	0	0	0	0
(200)	0(40)	105(12)	4	4	33	125
(121) (002) (210)	215(15)	597(21)	249	270	322	621
(210)	27(10)	40(13)	75	98	75	39
(012) (030) (201)	359(7)	660(12)	779	789	777	774
(102)	243(6)	217(10)	218	217	215	220
(211)	331(5)	304(9)	310	307	306	313
(112) (130) (031) (220)	4930(4)	4842(10)	4854	4820	4805	4898
(022)	3740(3)	3712(5)	3628	3612	3596	3661
(131) (221)	1127(4)	1330(7)	1328	1353	1315	1299
(122)	230(6)	220(11)	221	221	218	223
(202)	773(5)	821(9)	843	842	851	931
(300) (212) (040) (230)	1671(4)	1838(9)	1768	1842	1748	1819

Table 7. Discrepancy factors associated with the different models for $T = 1.5$ K.

$T = 1.5$ K Solution	Mn $(C_x, 0, 0)$	Mn $(C_x, C_y, 0)$	Mn $(C_x, F_y, 0)$	Mn $(C_x, F_y, 0)$	Nd $(0, F_y, 0)$
m_x	2.92(3)	2.90(4)	2.95(3)	2.89(3)	—
m_y	—	−0.21(13)	−1.34(12)	−1.44(18)	−1.24(18)
$\|m\|$	2.92(3)	2.91(3)	3.24(6)	3.22(9)	1.24(18)
R_{Bragg}	5.40	5.40	5.70	3.50	
χ^2	2.30	2.30	2.30	1.30	

the y-direction. In the thermal evolution of the NPD patterns the onset of a magnetic ordering is clearly observed at around $T = 78$ K, whereas no anomalies are observed in the zero-field-cooled magnetization curve at that temperature. However, a maximum is observed at around 60 K. Probably the fact that the curve was obtained under a 0.2 T magnetic field gave rise

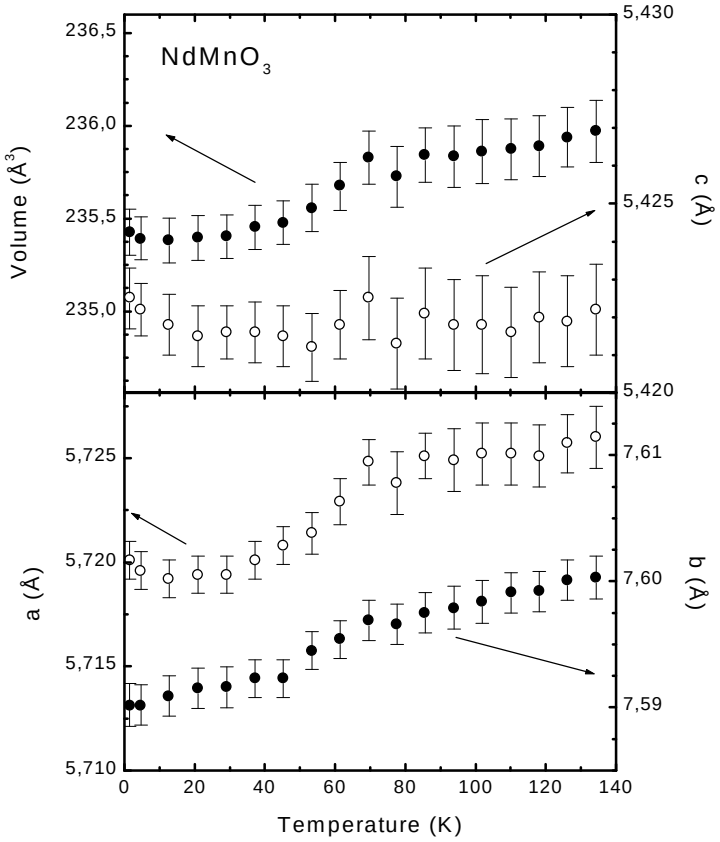

Figure 11. Thermal evolution of the lattice parameters.

to the shift of the transition to a lower temperature. On the other hand, the paramagnetic temperature calculated from the thermal evolution of the reciprocal susceptibility is -37 K, suggesting the presence of antiferromagnetic exchange interactions. This value, obtained in the temperature range 100–200 K, contrasts with the value given by Pauthenet and Veyret [6], $\Theta_P = 45$ K, obtained for the temperature range 300–750 K, tending to confirm the presence of ferromagnetic interactions in $NdMnO_3$. As is shown by Pauthenet and Veyret [6], the curvature observed in the inverse of the susceptibility at high temperatures is also observed in $SmMnO_3$ and $EuMnO_3$, but not in $GdMnO_3$, $TbMnO_3$ and $DyMnO_3$. As suggested by these authors [6], this effect can be associated with the Van Vleck paramagnetism given rise to by the action of the crystal field on the rare-earth ion.

The ordered magnetic moment obtained from neutron diffraction measurements at $T = 1.5$ K, 3.22(9) μ_B, is slightly lower than expected for Mn atoms in the trivalent oxidation state Mn^{3+} with $S = 2$ (ordered moment 4 μ_B). This probably means that the Mn moments are not completely ordered at 1.5 K (or there is an intrinsic disorder due to defects in the solid), but it could also be due to the presence of some mixed valence, Mn^{3+}–Mn^{4+} ($S = 3/2$ for Mn^{4+}). Although the refinement of the Nd occupancy factor from the high-resolution NPD data seems to exclude the metal non-stoichiometry that, in undoped manganese perovskites, has been shown to be responsible for the incrementing of the Mn oxidation state, the possibility of the presence of minor amounts of Mn^{4+} in this perovskite should not be ignored. As

regards the magnetic structure, our results are in contrast with preliminary findings of Quezel-Ambrunaz [14], who described it in terms of C_xC_y-modes (space group $Pnma$), and there was no evidence of magnetic ordering for Nd moments. Our data show that, when cooling, the Mn sub-lattice becomes firstly ordered and, at lower temperature, the rare-earth moments also adopt an ordered arrangement. Something similar has been described as occurring in $TbMnO_3$ [15]. The fact that the Nd sub-lattice becomes ordered according to the basis functions of the same irreducible representation as the Mn sublattice implies that the Nd-sub-lattice ordering is probably initiated by the local magnetic field created by the ordered Mn^{3+} moments at the Nd site. The Nd atoms are placed in the $y = \frac{1}{2}$ and $y = \frac{3}{4}$ planes, between two symmetric planes of Mn atoms. With respect to the x-component, both Mn layers are antiferromagnetically coupled; thus, this would give way to a zero magnetic field at the Nd site. Therefore, it is the ferromagnetic y-component of the Mn atoms that gives rise to a non-zero magnetic field at the Nd site and which is the responsible for the Nd-sub-lattice ordering. In $NdMnO_3$ the magnetic structure of the Mn sub-lattice is similar to that found for $LaMnO_3$, except for the presence of a ferromagnetic component along the y-direction in $NdMnO_3$. The fact of the lattice parameters obeying the relation $b/\sqrt{2} \leqslant c \leqslant a$, as well as the distribution of Mn–O distances, suggest that the distortion of the MnO_6 octahedra caused by the cooperative Jahn–Teller effect is also similar to that discerned in $LaMnO_3$. Therefore, the same arguments as were given to explain the observed magnetic structure in $LaMnO_3$ [13], namely the Goodenough–Kanamori rules [22, 23], will be invoked here. In the (x, z) plane the Mn atoms interact through two superexchange Mn–O2–Mn paths for which a ferromagnetic superexchange interaction between the Mn atoms is expected. In the interaction between (x, z) planes along the y-direction, only one Mn–O1–Mn path takes part, and for this path the Goodenough–Kanamori rules give an antiferromagnetic superexchange interaction. In $NdMnO_3$ there must also be additional ferromagnetic interactions between (x, z) planes in order to explain the ferromagnetic component in the magnetic moment of the Mn atoms along the y-direction. Perhaps the presence of minor amounts of Mn^{4+} could introduce an additional non-negligible ferromagnetic term via double exchange as described for hole-doped manganite perovskites. Probably the fact that the Goodenough–Kanamori rules are not totally followed in the Mn–O–Mn bond along the y-direction (the d orbitals are less than half-filled and the Mn–O–Mn bond angle is less than 180°, and also significantly lower than that found in $LaMnO_3$, of 155°) and the presence of Nd atoms with a magnetic moment that can introduce additional exchange interactions could give rise to the ferromagnetic component. A recent study carried out on $NdMnO_3$ and $LaMnO_3$ with a perturbed-angular-correlation spectroscopy technique [24] has shown some differences in the magnetic hyperfine field and in the electric field gradients at the Mn sites in the ordered regions of the two compounds. Therefore, a deeper study seems to be necessary in order to explain the appearance of a ferromagnetic component in the Mn atoms along the y-direction in the $NdMnO_3$ magnetic structure.

6. Conclusions

Neutron diffraction measurements have shown that $NdMnO_3$ orders below $T_N \approx 78$ K with a commensurable magnetic structure. Firstly, in the temperature range immediately below T_N, only the Mn sub-lattice becomes ordered with a spin arrangement $(C_x, F_y, 0)$. Subsequently, a ferromagnetic component appears along the y-direction. As temperature decreases both components of the magnetic moments increase, giving rise to a canting of the moments in the (x, y) plane. Secondly, the polarization effects at the Nd sites lead to the Nd sub-lattice ordering below $T \approx 13$ K with a ferromagnetic structure parallel to the y-direction. At $T = 1.5$ K the magnetic moment values are 3.22(9) μ_B for Mn atoms and 1.2(2) μ_B for Nd atoms.

References

[1] Von Helmolt R, Wecker J, Holzapfel B, Schultz L and Samwer K 1993 *Phys. Rev. Lett.* **71** 2331
[2] Chahara K, Ohno T, Kasai M and Kozono Y 1993 *Appl. Phys. Lett.* **63** 1990
[3] Jim S, Tiefel T H, McCormack M, Fastnacht R, Ramesh R and Chen J H 1994 *Science* **264** 413
[4] Jonker G J and Van Santen J H 1950 *Physica* **16** 337
[5] Jonker G J 1956 *Physica* **36** 707
[6] Pauthenet R and Veyret C 1970 *J. Physique* **31** 65
[7] Kuwahara H, Tomioka Y, Asamitsu A, Moritomo Y and Tokura Y 1995 *Science* **270** 961
[8] Tomioka Y, Asamitsu A, Kuwahara H, Moritomo Y and Tokura Y 1996 *Phys. Rev.* B **53** R1689
[9] Yoshizawa H, Kawano H, Tomioka Y and Tokura Y 1996 *J. Phys. Soc. Japan* **65** 1043
[10] Gilleo M A 1957 *Acta Crystallogr.* **10** 161
[11] Wollan E O and Koehler W C 1955 *Phys. Rev.* **100** 545
[12] Koehler W C and Wollan E O 1957 *J. Phys. Chem. Solids* **2** 100
[13] Moussa F, Hennion M, Rodríguez-Carvajal J, Moudden H, Pinsard L and Revcolevschi A 1996 *Phys. Rev.* B **54** 15 149
[14] Quezel-Ambrunaz S 1968 *Bull. Soc. Fr. Minéral. Cristallogr.* B **91** 339
[15] Quezel S, Tcheou F, Rossat-Mignod J, Quezel G and Roudaut E 1977 *Physica* B **86–88** 916
[16] Mukovski Y M, Hilscher G, Michor H and Ionov M 1998 *J. Appl. Phys.* **83** 7163
[17] Troyanchuk I O, Sumsonenko N V, Kasper N V, Szymczak H and Nabialek A 1997 *J. Phys.: Condens. Matter* **9** 8287
[18] Rietveld H M 1969 *J. Appl. Crystallogr.* **2** 65
[19] Rodríguez-Carvajal J 1993 *Physica* B **12** 55
[20] *International Tables for Crystallography* 1992 vol C, ed A J C Wilson (London: Kluwer-Academic) p 391
[21] Bertaut E F 1968 *Acta Crystallogr.* A **24** 217
[22] Goodenough J B 1955 *Phys. Rev.* **100** 564
[23] Kanamori J 1959 *J. Phys. Chem. Solids* **10** 87
[24] Rasera R L and Catchen G L 1998 *Phys. Rev.* B **58** 3218